Modelling of aerosol deposition in human lungs

Diederik Kokkedee

Double degree Bachelor Thesis
Applied Physics
Applied Mathematics

Delft, 7 february 2022

BEP
TNW
TU Delft

Supervisors: Prof. Dr. S. Kenjereš
Prof. Dr.ir. K.C. Vuik
Dr.ir. J.M. Thijssen
Prof. Dr. H.M. Schuttelaars

Contents

Abstract

A one-dimensional model of respiratory deposition is developed based on an Eulerian approach. The model simulates aerosol deposition in all generations of the respiratory tract by numerically solving the aerosol general dynamics equation (GDE) for a range of aerosol diameters. The lung geometry is described by Weibel's morphometric model, with a time varying alveolar geometry to accommodate inhalation dynamics. The model is first valuated by comparing it with numerical and experimental results. Afterwards a series of parameter studies is performed by changing breathing conditions, particle parameters and lung geometries. An increase in Tidal volume and decrease of breathing period resulted in an increase of the total deposition fraction for coarse particles and a decrease of the total deposition fraction for ultrafine particles. An increase in the particle density resulted in an increase in the total deposition fraction. A decrease in the airway diameter generally resulted in an increase of the total deposition fraction. This difference was most noticeable in the tracheobronchial region. Decreasing the airway diameter in the tracheobronchial region mostly effects coarse particles while decreasing the airway diameter in the alveolar region mostly effects ultrafine particles.

1. Introduction

Aerosols are minute particles suspended in the atmosphere. When these particles are sufficiently large, their presence is noticed as they scatter and absorb sunlight. Examples of natural aerosols are fog or mist, dust, forest exudates, and geyser steam. Examples of anthropogenic aerosols are particulate air pollutants and smoke. So aerosols have been around for a very long time but in the last two years they have gotten extra attention: the SARS-CoV-2, or coronavirus, spreads through aerosols in the air. That is the main reason why the whole world had to go into lockdown.

The purpose of the present work is to create a whole respiratory tract (RT) computational deposition model. The estimation of the aerosol deposition and its distribution in the RT during breathing is of importance in environmental health and occupational hygiene assessments. By creating a mechanistic computational model one can calculate respiratory deposition on the basis of realistic description of lung structure and physiology, and as a result of physical processes. The essential benefit of mechanistic modelling is the ability to address a variety of conditions. For example, it is possible to investigate variations in breathing patterns, or effects connected with the respiratory tract morphology.

The model will be based around a one-dimensional Eulerian approach developed by Mitsakou et al. [1] This is possible by considering the lungs as a one-dimensional model based on idealized descriptions of lung geometry, Weibel's scheme [2]. The advantage of creating a one-dimensional model over a computationally intensive model based on computational fluid dynamics is that it is possible to analyse the whole RT, instead of single elements in isolation from the rest of the system. Besides, a one-dimensional model will have a short running time allowing determination of deposition for particles of different sizes under a range of respiratory conditions.

The model will be validated by comparing extensively with measurements and previous numerical results. Since the model is based on generic mechanistic principles, favourable validation will provide confidence to apply the model over a variety of exposure scenarios and conditions. Hence, contrary to empirical models the present model may eventually be used for extrapolation beyond the range in which measurements are available. This will be done in a series of parameter studies. The deposition fraction will be determined for different breathing conditions, particle parameters and lung geometries.

Chapter 2 of this report will describe the lung model and introduces the mechanic of aerosol dynamics. In Chapter 3 the equation describing the mechanics of aerosol will numerically be solved. Also convergence of this equation will be shown. Chapter 4 will start with the validation of the model with experimental en previous numerical results. After that a series of parameters studies analysing the influence of different breathing conditions, particle parameters and lung morphology's to the deposition fraction. Finally, chapter 5 describes the conclusions of this study and gives some recommendations.

2. Theory

The goal of this section is to give information about lung models and aerosol dynamics. First the one-dimensional lung geometry and respiration model will be explained. After that aerosol dynamics will be discussed and this section will conclude with explanation about the velocity profile and deposition fraction.

2.1. Weibel Model

The long model used in this report is the model made by E.R. Weibel in 1963, called model 'A' [2]. This is one of the simplest and widely used models of the human lung. The symmetrical geometrical structure described by Weibel starts at the trachea and splits into two bronchi called the primary bronchi. These two primary bronchi split again into four secondary bronchi. The trachea is generation 0 and every time a bronchi splits a generation is added. This splitting continues until the 23rd generation, see figure 1. Generation 0 up to 16 are conducting airways, this region is called the tracheobronchial regoin. Whilr generation 16 up to generation 23 are acinar airways, this region is called the alveolar region. The difference between these two zones is that the bronchi in the respiratory zone have alveoli attached to them. Alveoli are small pockets where gas exchange takes place. The number of bronchi per generation can be

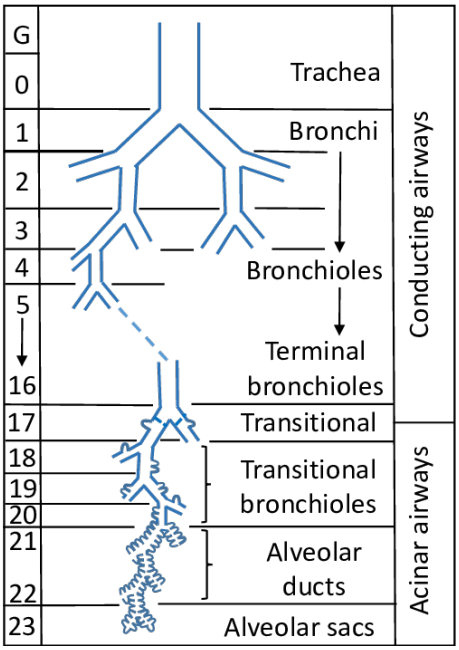

Figure 1: Schematic representation of geometrical structure of the lungs [3]

calculated as 2^n with n the generation number. This results in $2^{23} = 8388608$ bronchi in the last generation. Besides the number of airways per generation, Weibel's model also specifies what the length and diameter of the airways are in each generation. As stated before, the Weibel's model is a symmetric model, resulting in constant branching and gravitational angles for all generations. Where the branching angle is the angle between parent and daughter airway and the gravitational angle is the angle between the airway direction and the force of gravity. In Weibel's model the gravitational and branching angle are respectively given by 45° and 60°. All

this together results in a 1-dimensional lung model; when the distance from the trachea is given, Weibel's model gives the amount of airways, airway diameter and length and gravitational and branching angle. For the values of the airway diameter and length in Weibel's model, see Table 1 in the Appendix.

2.2. Respiration model

Respiration is the process of moving air in the lungs to facilitate the absorption of oxygen and removal of carbon dioxide. This is done by contraction of the diaphragm and pulling upwards and outwards of the rib cage. During normal breathing, the volume of air inhaled or exhaled in one breath is called the tidal volume V_T. After normal passive exhaling there is still air left in the lungs, the functional residual capacity V_{FRC}. See Figure 2 for a schematic representation of the different volumes during breathing.

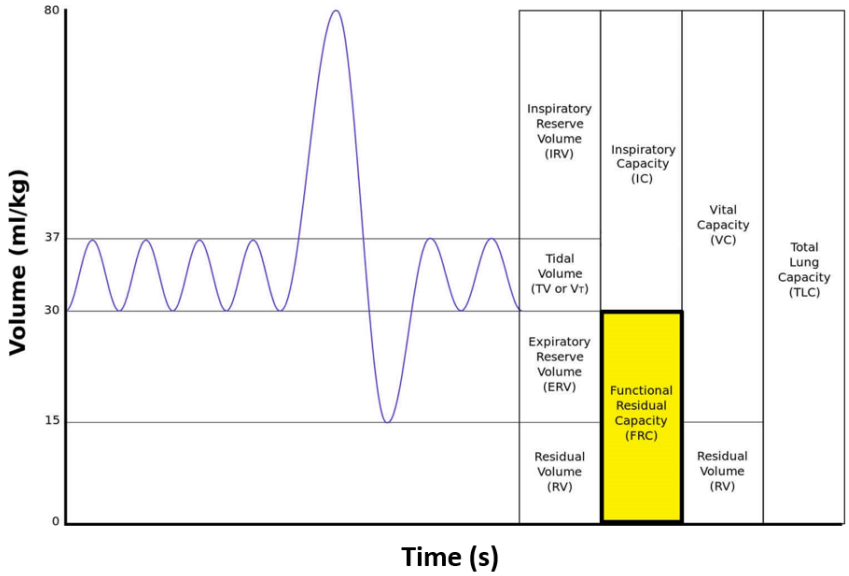

Figure 2: Schematic representation of different lung volumes during breathing. Pay special attention to the tidal volume and functional residual capacity, these will be important in the rest of this report.

The volume of the alveolated section of the lung is let to vary with time to accommodate effects due to breathing dynamics. The mean value of the lung volume during a breathing cycle is taken to be equal to the functional residual capacity plus one-half of the tidal volume. Hence, lung volume is considered to vary with times as

$$V_{\mathrm{L}} = \left(V_{\mathrm{FRC}} + \frac{V_{\mathrm{T}}}{2} \right) + \frac{V_{\mathrm{T}}}{2} f(t) \tag{1}$$

where $f(t)$ is a function of time that takes values between 1 (end of inspiration) and -1 (end of expiration). In this report symmetric two-phase breathing is assumed; $f(t)$ is specified by a sinusiodal function. More precisely, $f(t) = -\cos(2\pi t/T)$ where T represents the breathing period. A time-varying alveolar geometry is employed to accommodate inhalation dynamics

so that that the diameter of the alveolated airways are given by

$$\frac{d_{\mathrm{T}}}{d_{\mathrm{A}}} = \left(\frac{V_{\mathrm{L}}}{V_{\mathrm{FRC}}}\right)^{1/3} \text{ for generations } \geqslant 16 \tag{2}$$

2.3. Aerosol Dynamics

Different processes, acting simultaneously determine the transport of the inhaled matter, such as aerosols. All these process together are described by the aerosol general dynamic equation (GDE), which is considered in a one-dimensional form along the flow direction (from the trachea to the bottom/end of the lungs). The GDE is given as [1]

$$\begin{aligned}\frac{\partial}{\partial t}(A_T N_i) = -\frac{\partial}{\partial x}(A_A u N_i) + \frac{\partial}{\partial x}\left(A_T D_{eff_i}\frac{\partial N_i}{\partial x}\right) - V_{d_i}\Gamma N_i + (\frac{\partial}{\partial t}(A_T N_i))_{growth} \\ + (\frac{\partial}{\partial t}(A_T N_i))_{coagulation}\end{aligned} \tag{3}$$

The goal of this project is to determine $N(x,t)$, the particle or aerosol concentration, for all x in the lungs and t during a breathing period. Note that the subscript i in equation 4 presents the particle size. In equation 4 A_A corresponds to the time independent cross-sectional area of all airways at distance x from the trachea. Section 2.1 showed that Weibel's model describes the airway diameter $d_A(x)$ and total number of airways $n(x)$ for each x inside the lungs. Then the total time independent cross-sectional area is given by $A_A(x) = n\pi d_A^2/4$. Section 2.2 showed that a time-varying alveolar geometry is employed to accommodate inhalation dynamics resulting in a time dependent diameter d_T. From this it follows that the total time dependent cross-sectional area is given by $A_T(x,t) = n\pi d_T^2/4$.

The first term on the right-hand side of equation 4 is the convective term, which describes how particles behave due to bulk motion of a fluid or air. This term depends on u which corresponds to the velocity of the air in the lungs due to breathing. Convective transport is assumed to occur through the cross-sectional area corresponding to the airways alone and not through the part corresponding to the alveoli. Hence the convective term is proportional to A_A

The second term on the right hand side corresponds to the Brownian diffusion term, which describes the random motion of particles suspended in a medium. This motion is always a net flow of matter from a region of high concentration to a region of low concentration. Unlike the convective term, diffusion is assumed to occur through the cross-sectional including alveoli, hence the diffusion term is proportional to A_T. In the absence of convective flow, the transport of particles in lungs would be controlled by Brownian diffusion alone. Convective aerosol flow changes direction periodically during inspiration and expiration and as a result, a complicated flow pattern is developed, accompanied by bulk irreversible mixing between tidal volume and reserved air. Scherer et al [4] investigated experimentally these effects in the first generations of Weibel's geometry and proposed an effective diffusion coefficient to account for bulk mixing. This coefficient, different for inspiration and expiration, is given below

$$D_{\text{eff}} = \begin{cases} D_{\mathrm{B}} + 1.08 \cdot u \cdot d_{\mathrm{T}} & \text{for inspiration,} \\ D_{\mathrm{B}} + 0.37 \cdot u \cdot d_{\mathrm{T}} & \text{for expiration.} \end{cases} \tag{4}$$

The Brownian diffusion coefficient D_B is determined from the Stokes-Einstein equation [5]

$$D_{\mathrm{B}} = \frac{k_{\mathrm{B}} T_{\mathrm{g}} C_{\mathrm{c}}}{3\pi \mu_{\mathrm{g}} d} \tag{5}$$

In which d is the particle diameter, k_B is Boltzmann's constant, T_G the temperature of air in the lungs and C_c the Cunningham's correction factor which is used to account for noncontinuum effects. The latter is given as [6]

$$C_c = 1 + \frac{2\lambda}{d}\left(A_1 + A_2 \cdot \exp\frac{-A_3 d}{\lambda}\right) \tag{6}$$

where for air: $A_1 = 1.257$, $A_2 = 0.400$ and $A_3 = 0.55$. Note that Cunningham's correction factor also depends on the particle diameter d and the mean free path λ. The latter is taken as $\lambda = 68$nm [7].

The third term on the right hand side describes the deposition of particles in the lungs. This is the process of spontaneous attachment of particles to the surface of the lungs. Deposition of particles is linear with the concentration and is influenced by two terms. Firstly the wetted perimeter, which is given as $\Gamma = n\pi d_T$. Note that d_T varies with time in the alveolated part of the lungs, so Γ is also a function of time. Secondly by the deposition velocity V_d, which is given as the sum of the deposition velocities corresponding three different effects, namely $V_d = V_{d(sed)} + V_{d(dif)} + V_{d(imp)}$.

The deposition velocity due to gravitational settling is given as

$$V_{\mathrm{d(sed)}} = u_{\mathrm{s}} \sin\theta \tag{7}$$

where $u_s = \rho_p d^2 g C_c / 18\mu$ is the terminal settling velocity as determined from the Stokes' law for the drag force, ρ_p represents the particle density, $g = 9.81\frac{m}{s^2}$ the gravity acceleration and $\mu = 1.81 \cdot 10^{-5}\frac{kg}{m \cdot s}$ the viscosity of air. The angle θ is the gravity angle, which is the angle between the airway direction and the force of gravity. The gravity angle is taken from Weibel's data. The term sin θ is included so that deposition flux is correctly attributed to a fraction of the inner airway surface, since sedimentation is a directional mechanism.

The deposition velocity due to Brownian diffusion is determined from mass transfer theory and given by

$$V_{\mathrm{d(dif)}} = \frac{D_{\mathrm{B}} Sh}{d_{\mathrm{T}}} \tag{8}$$

The local Sherwood number Sh is specified as a function of the distance from the beginning of the airway to properly account for entrance effects. The Sherwoord number can be written as a function of the dimensionless length $x^+ = x/d_T ReSc_p$ [8]:

$$\mathrm{Sh}\left(x^+\right) = \begin{cases} 1.077\left(x^+\right)^{-1/3} - 0.7 \text{ for } x^+ \leqslant 0.01 \\ 3.657 + 6.874\left(10^3 x^+\right)^{-0.488}\exp\left(-57.2x^+\right) \quad \text{for } x^+ > 0.01 \end{cases} \tag{9}$$

where the Reynolds number is given by [9]

$$Re = \frac{\rho_a u d_T}{\mu} \tag{10}$$

and Schmidt's number is given by [10]

$$Sc = \frac{\mu}{\rho_a D_B}. \tag{11}$$

Note that $\rho_a = 1.23 \frac{kg}{m^3}$ represents the density of air.

Deposition due to inertial effects, or impaction, is determined on the basis of a simplified analysis of the curvilinear motion in the airway bifurcation region and can be expressed as follows [11]:

$$V_{\mathrm{d(imp)}} = \begin{cases} 0 \text{ (over the first } 80\% \text{ of the airway length)}, \\ Stk'u = Stku\phi d_{\mathrm{T}}/0.2L \text{ (over the last } 20\% \text{ of the airway length)} \end{cases} \tag{12}$$

Where ϕ represents the branching angle, which is the angle between parent and daughter airway. The Stokes number is given by [12]:

$$\mathrm{Stk} = \frac{t_0 u}{d_T} \tag{13}$$

where t_0 is the relaxation time, given by

$$t_0 = \frac{\rho_p d^2 C_c}{18 \mu_g}. \tag{14}$$

The last two terms in equation 4 present the growth and coagulation term. These will be not be considered in this report. Only situations in which all the particles have the same diameter will be analysed.

2.4. Velocity

In order to solve the GDE the velocity along the airways in the respiratory tract has to been known. The velocity is determined by solving the equation of continuity which states that the rate at which mass enters a system is equal to the rate at which mass leaves the system. The previous section explained that convective transport is assumed to occur through the cross-sectional area corresponding to the airways alone, hence the flux in any airway is given by $A_A u$. Now since a time-varying alveolar geometry is employed to accommodate inhalation dynamics and a constant density is assumed, the continuity equation is given as [1]:

$$\frac{\partial A_T}{\partial t} = -\frac{\partial \left(A_A u\right)}{\partial x} \tag{15}$$

This equation can be rewritten if a (one-dimensional) volume is considered with $x = a$ on the upper side of the lung and $x = b$ at the lower side of the volume.

$$\int_a^b \frac{\partial}{\partial t} A_T dx = -u A_A|_a^b$$

Solving this for u yields,

$$u(b,t) = \frac{1}{A_A(b)} \left(u(a,t) A_A(a) - \int_a^b \frac{\partial}{\partial t} A_T(x,t) dx \right) \tag{16}$$

Now the velocity $u(x,t)$ can be calculated everywhere in the respiratory tract. The inlet velocity is simply $u(0,t) = \frac{\partial}{\partial t} V_L(t)/A_A(0)$. Note that for generations smaller than 16, $A_T = A_A$ and thus $\frac{\partial A_T}{\partial t} = 0$ so that $u(b,t) = u(a,t)A_A(a)/A_A(b)$.

2.5. Deposition fraction

By solving the GDE it is possible to determine the aerosol concentration as function of time along the whole respiratory tract. Hence, the model permits to track the changes of the concentration throughout the whole respiratory tract during a breathing cycle. The deposited fraction in a specific area of the lung with length L (for example, a generation) is determined as the fraction of the number of particles deposited in the area to the number of particles that are introduced in the RT. The number of particles (with diameter index i) deposited in a certain area with length L can be calculated as $\int_0^T \int_0^L N_i n V_{\mathrm{d}_i} \Gamma \mathrm{d}x \, \mathrm{d}t$. Note that the integration is over a whole breathing cycle. The total number of particles that are introduced in the RT can be calculated as $\int_0^{T/2} N_{i0} A_{\mathrm{A}_0} u_0 \, \mathrm{d}t$ where the time integration is only over half a breathing period, the inspiration phase. Consequently the deposition fraction can be calculated as [1]

$$\text{deposition fraction } = \frac{\int_0^T \int_0^L N_i n V_{\mathrm{d}_i} \Gamma \mathrm{d}x \, \mathrm{d}t}{\int_0^{T/2} N_{i0} A_{\mathrm{A}_0} u_0 \, \mathrm{d}t} \tag{17}$$

where A_{A_0} is the cross-sectional area of the entrance and u_0 the air velocity at the entrance.

3. Numerics

This section starts with developing a numerical scheme to solve the GDE, equation (4). This will be done with the finite volume method. Afterwards the convergence of the numerical solution will be investigated.

3.1. Finite Volume

Recall that the GDE, equation (4), without the growth and coagulation term is given by:

$$\frac{\partial}{\partial t}(A_T N_i) = -\frac{\partial}{\partial x}(A_A u N_i) + \frac{\partial}{\partial x}(A_T D_{eff_i} \frac{\partial N_i}{\partial x}) - V_{d_i} \Gamma N_i \tag{18}$$

To simplify the equation the following are substituted: $\alpha = A_T$, $\beta = A_T D_{eff}$, $\gamma = A_A u$ and $\epsilon = V_d \Gamma$. Now write q as the aerosol concentration (instead of N), to get a standard form:

$$\frac{\partial}{\partial t}(\alpha q) = -\frac{\partial}{\partial x}(\gamma q) + \frac{\partial}{\partial x}\left(\beta \frac{\partial q}{\partial x}\right) - \epsilon q \tag{19}$$

In one space dimension, a finite volume method is based on subdividing the spatial domain into intervals (grid cells) and keeping track of an approximation to the integral of q over each of these volumes. In each time step we update these values using approximation to the flux through the endpoints of the intervals.

Denote the ith grid cell by

$$\mathcal{C}_i = \left(x_{i-1/2}, x_{i+1/2}\right) \tag{20}$$

The value Q_i^n will approximate the average value over the ith interval at time t_n [13]:

$$Q_i^n \approx \frac{1}{\Delta x_i} \int_{x_{i-1/2}}^{x_{i+1/2}} q\left(x, t_n\right) dx \equiv \frac{1}{\Delta x_i} \int_{\mathcal{C}_i} q\left(x, t_n\right) dx \tag{21}$$

where $\Delta x_i = x_{i+\frac{1}{2}} - x_{i-\frac{1}{2}}$ is the length of the cell.

Integrating (19) over a grid cell gives

$$\frac{d}{dt} \int_{x_{i-1/2}}^{x_{i+1/2}} \alpha q(x,t) dx = f\left(q\left(x_{i-1/2}, t\right)\right) - f\left(q\left(x_{i+1/2}, t\right)\right) - \int_{x_{i-1/2}}^{x_{i+1/2}} \epsilon q(x,t) dx$$

where f is the flux function which is given by $f(q, q_x, x) = \gamma(x) q - \beta(x) q_x$. Now the θ-method will be used for time integration from t^n to t^{n+1} to get a mixed implicit/explicit scheme. Note that for $\theta = 0$ the equation is fully explicit, for $\theta = 1$ fully implicit, and for $\theta = \frac{1}{2}$ the so called Crank-Nicolson method is obtained.

$$\begin{aligned} \alpha_i^{n+1} Q_i^{n+1} = \alpha_i^n Q_i^n + \frac{\Delta t}{\Delta x_i} \big[&(1-\theta)\left(F_{i-1/2}^n - F_{i+1/2}^n - \Delta x_i \epsilon Q_i^n\right) \\ &+ \theta(F_{i-1/2}^{n+1} - F_{i+1/2}^{n+1} - \Delta x_i \epsilon Q_i^{n+1}) \big] \end{aligned} \tag{22}$$

Where $F_{i-\frac{1}{2}}^n$ is some approximation to the average flux along $x = x_{i-\frac{1}{2}}$, given by:

$$F_{i-1/2}^n \approx \frac{1}{\Delta t} \int_{t_n}^{t_{n+1}} f\left(q\left(x_{i-1/2}, t\right)\right) dt \tag{23}$$

Given two cell averages Q^n_{i-1} and Q^n_i , the numerical flux $F^n_{i-1/2}$ at the cell interface between can very naturally be defined as

$$F^n_{i-1/2} = -\beta^n_{i-1/2}\left(\frac{Q^n_i - Q^n_{i-1}}{\Delta x_{i-1/2}}\right) + \gamma^n_{i-1/2}Q^n_{i-1} \tag{24}$$

Where $\beta_{i-1/2} \approx \beta(x_{i-1/2})$ and $\Delta x_{i-1/2} = x_i - x_{i-1}$. For the diffusion term a central difference scheme has been used while for the advection central difference would result in non physical solutions. Instead, the upwind scheme is used for the advection term during inspiration and downwind during expiration. Same can be done for $F^n_{i+1/2}$, $F^{n+1}_{i-1/2}$ and $F^{n+1}_{i+1/2}$ to get the following solution for inspiration:

$$\begin{aligned}\alpha^{n+1}_i Q^{n+1}_i = \alpha^n_i Q^n_i + \frac{\Delta t}{\Delta x_i}\Bigg[&(1-\theta)\left(-\beta^n_{i-1/2}\left(\frac{Q^n_i - Q^n_{i-1}}{\Delta x_{i-1/2}}\right) + \gamma^n_{i-1/2}Q^n_{i-1} - \Delta x_i \epsilon Q^n_i\right)\\ &-(1-\theta)\left(-\beta^n_{i+1/2}\left(\frac{Q^n_{i+1} - Q^n_i}{\Delta x_{i+1/2}}\right) + \gamma^n_{i+1/2}Q^n_i\right)\\ &+\theta\left(-\beta^{n+1}_{i-1/2}\left(\frac{Q^{n+1}_i - Q^{n+1}_{i-1}}{\Delta x_{i-1/2}}\right) + \gamma^{n+1}_{i-1/2}Q^{n+1}_{i-1} - \Delta x_i \epsilon Q^{n+1}_i\right)\\ &-\theta\left(-\beta^{n+1}_{i+1/2}\left(\frac{Q^{n+1}_{i+1} - Q^{n+1}_i}{\Delta x_{i+1/2}}\right) + \gamma^{n+1}_{i+1/2}Q^{n+1}_i\right)\Bigg]\end{aligned} \tag{25}$$

This equation can be written in matrix form. For that $\boldsymbol{Q}^n$ now represent a vector with the solution at any x in the lungs and at time step t^n.

$$\boldsymbol{Q}^{n+1} = \boldsymbol{Q}^n + \frac{\Delta t}{\Delta x}\left[(1-\theta)\left(\mathbf{A}^n\boldsymbol{Q}^n + \mathbf{b}^n\right) + \theta\left(\mathbf{A}^{n+1}\boldsymbol{Q}^{n+1} + \mathbf{b}^{n+1}\right)\right] \tag{26}$$

where Δx is a vector with all Δx_i values. $\boldsymbol{A}$ is a tridiagonal matrix with (for inspiration) $-\beta^n_{i-1/2}/\Delta x_{i-1/2} - \beta^n_{i+1/2}/\Delta x_{i+1/2} + \gamma^n_{i+1/2} - \Delta x_i\epsilon$ on the center diagonal (the Q^n_i position), $\beta^n_{i-1/2}/\Delta x_{i-1/2} + \gamma^n_{i-1/2}$ on the left diagonal (the Q^n_{i-1} position) and $\beta^n_{i+1/2}$ on the right diagonal (the Q^n_{i+1} position). $\boldsymbol{b}$ is a vector which has values due to boundary conditions. Section 3.2 explains which boundary conditions are used and what effect they have on the matrix $\boldsymbol{A}$ and vector $\boldsymbol{b}$. Equation (26) can be rewritten in an explicit way:

$$\boldsymbol{Q}^{n+1} = \left(I - \frac{\Delta t}{\Delta x}\theta\mathbf{A}^{n+1}\right)^{-1}\left[\left(I + \frac{\Delta t}{\Delta x}(1-\theta)\mathbf{A}^n\right)\boldsymbol{Q}^n + \frac{\Delta t}{\Delta x}\left((1-\theta)\mathbf{b}^n + \theta\mathbf{b}^{n+1}\right)\right] \tag{27}$$

With this equation the aerosol concentration can be calculated iteratively for every moment in a breathing period and every generation in the lungs.

3.2. Mesh description

The previous section showed that the GDE can numerically be solved with equation (27). For this N equally spaced nodes will be distributed in every generation of Weibels model, with one extra in the first generation. This results in a total grid size of $24N$+1 nodes. Now since the airway length differs per generation, the distance Δx between the nodes will also differ per generation. Generally, a larger grid size produces more accurate results than a smaller grid size. In section 4 this dependency will be investigated.

3.3. Boundary and Initial conditions

The initial value of the aerosol concentration in the whole respiratory tract is specified to zero (t = 0, $N_i = 0$). Boundary conditions need to be specified at the entrance and the end of the respiratory tract. During inspiration, the concentration at the entrance is given a specified value. It does not matter what this concentration value is, so for $x = 0$ and $0 < t < T/2$, $N_{i0} = 1$ will be used. This type of boundary conditions is known as a Dirichlet boundary condition. Since the concentration is given at the boundary the value can directly be substituted in equation (25). Doing so results in a term in the first element of vector $\boldsymbol{b}$.

During expiration, the normal derivative at the entrance is taken as zero, namely, at $x = 0$ and $T/2 < t < T$, $\partial N_i/\partial x = 0$. This type of boundary condition is known as a Neumann boundary condition. The latter is the usual condition employed on outflow boundaries where a smooth continuation in the flow transported out of the computational domain is assumed. Unlike Dirichlet boundary conditions, Neumann boundary conditions cannot directly be substituted. Instead, since the flux is given at x=0 and assume $F_{0-1/2} = F_0 = 0$ which can be substituted directly in equation (22) resulting in an equation for Q_0.

At the end of the respiratory tract mass flux is zero. Hence, again, a zero concentration gradient is applied both during inspiration and expiration. This can be implemented in the same way as the Neumann boundary condition at the entrance during expiration with $F_{N+1/2} = F_N = 0$.

3.4. Convergence

There are several considerations that go into judging how good a particular flux function is for numerical computation. One essential requirement is that the resulting method should be convergent, i.e., the numerical solution should converge to the true solution of the differential equation as the grid is refined (as Δx, $\Delta t \to 0$). This generally requires two conditions [13]:

- The method must be consistent with the differential equation, meaning that it approximates it well locally.
- The method must be stable in some appropriate sense, meaning that the small errors made in each time step do not grow too fast in later time steps.

3.4.1. Consistency

A numerical solution is called consistent if the local truncation error goes to zero as Δt goes to zero [13]. The local truncation error is given by the error caused by one iteration. In general explicit numerical method can be written as $Q^{n+1} = \mathcal{N}(Q^n)$, where $\mathcal{N}(\cdot)$ represents the numerical operator mapping the approximate solution at one time step to the approximate solution at the next. The local truncation error is then defined as:

$$\tau^n = \frac{1}{\Delta t}\left[\mathcal{N}\left(q^n\right) - q^{n+1}\right] \tag{28}$$

So suppose a true solution is given by q_i^n and q_i^{n+1} then the truncation error after one iteration is given by (where constant coefficients and splitting of q_i^{n+1} is used for simplicity)

$$\begin{aligned}\tau_n =&\frac{1}{\Delta t}\left[(1-\theta)q_i^n + \frac{\Delta t}{\Delta x\alpha}(1-\theta)\left(\beta\frac{q_{i+1}^n - 2q_i^n + q_{i-1}^n}{\Delta x} + \gamma(q_{i-1}^n - q_i^n) - \Delta x\epsilon q_i^n\right) - (1-\theta)q_i^{n+1}\right.\\ &\left. + \theta q_i^n + \frac{\Delta t}{\Delta x\alpha}\theta\left(\beta\frac{q_{i+1}^{n+1} - 2q_i^{n+1} + q_{i-1}^{n+1}}{\Delta x} + \gamma(q_{i-1}^{n+1} - q_i^{n+1}) - \Delta x\epsilon q_i^{n+1}\right) - \theta q_i^{n+1}\right]\end{aligned}$$

Now expand q_{i-1}^n, q_{i+1}^n and q_i^{n+1} in Taylor series around q_i^n and expand q_{i-1}^{n+1}, q_{i+1}^{n+1} and q_i^n in Taylor series around q_i^{n+1}:

$$\begin{aligned}q_{i+1}^n &= q_i^n + \Delta x q_x^n + \frac{1}{2}\Delta x^2 q_{xx}^n + \mathcal{O}\left(\Delta x^3\right)\\ q_{i-1}^n &= q_i^n - \Delta x q_x^n + \frac{1}{2}\Delta x^2 q_{xx}^n + \mathcal{O}\left(\Delta x^3\right)\\ q_i^{n+1} &= q_i^n + \Delta t q_t^n + \mathcal{O}\left(\Delta t^2\right)\\ q_{i+1}^{n+1} &= q_i^{n+1} + \Delta x q_x^{n+1} + \frac{1}{2}\Delta x^2 q_{xx}^{n+1} + \mathcal{O}\left(\Delta x^3\right)\\ q_{i-1}^{n+1} &= q_i^{n+1} - \Delta x q_x^{n+1} + \frac{1}{2}\Delta x^2 q_{xx}^{n+1} + \mathcal{O}\left(\Delta x^3\right)\\ q_i^n &= q_i^{n+1} + \Delta t q_t + \mathcal{O}\left(\Delta t^2\right)\end{aligned}$$

Substituting these equations into the local truncation error results in:

$$\begin{aligned}\tau_n =&\frac{1}{\Delta t}\left[\frac{\Delta t}{\Delta x\alpha}(1-\theta)\left(\beta\frac{\Delta x^2 q_{xx}^n + \mathcal{O}\left(\Delta x^3\right)}{\Delta x} + \gamma(-\Delta x q_x^n + \mathcal{O}\left(\Delta x^2\right)) - \Delta x\epsilon q_i^n\right)\right.\\ &- (1-\theta)\left(\Delta t q_t^n + \mathcal{O}\left(\Delta t^2\right)\right)\\ &\left. + \theta\left(\Delta t q_t + \mathcal{O}\left(\Delta t^2\right)\right) + \frac{\Delta t}{\Delta x\alpha}\theta\left(\beta\frac{\Delta x^2 q_{xx}^{n+1} + \mathcal{O}\left(\Delta x^3\right)}{\Delta x} + \gamma(-\Delta x q_x^{n+1} + \mathcal{O}\left(\Delta x^2\right) - \Delta x\epsilon q_i^{n+1}\right)\right]\\ =&\frac{1}{\Delta t}\left[\frac{\Delta t}{\alpha}(1-\theta)\left(q_{xx}^n - \gamma q_x^n - \epsilon q_i^n + \mathcal{O}(\Delta x)\right) - (1-\theta)\left(\Delta t q_t^n + \mathcal{O}\left(\Delta t^2\right)\right)\right.\\ &\left. + \frac{\Delta t}{\alpha}\theta\left(q_{xx}^{n+1} - \gamma q_x^{n+1} - \epsilon q_i^{n+1} + \mathcal{O}(\Delta x)\right) - \theta\left(\Delta t q_t^{n+1} + \mathcal{O}\left(\Delta t^2\right)\right)\right]\end{aligned}$$

Now use that $q_{xx}^n - \gamma q_x^n - \epsilon q_i^n = \alpha q_t^n$ and $q_{xx}^{n+1} - \gamma q_x^{n+1} - \epsilon q_i^{n+1} = \alpha q_t^{n+1}$ to get:

$$\begin{aligned}\tau_n =&\frac{1}{\Delta t}\left[\frac{\Delta t}{\alpha}(1-\theta)\left(\alpha q_t^n + \mathcal{O}(\Delta x)\right) - (1-\theta)\left(\Delta t q_t^n + \mathcal{O}\left(\Delta t^2\right)\right)\right.\\ &\left. + \frac{\Delta t}{\alpha}\theta\left(\alpha q_t^{n+1} + \mathcal{O}(\Delta x)\right) - \theta\left(\Delta t q_t^{n+1} + \mathcal{O}\left(\Delta t^2\right)\right)\right]\\ =&\frac{1}{\Delta t}\left[\frac{\Delta t}{\alpha}(1-\theta)\mathcal{O}(\Delta x) - (1-\theta)\mathcal{O}(\Delta t^2) + \frac{\Delta t}{\alpha}\theta\mathcal{O}(\Delta x) - \theta\mathcal{O}(\Delta t^2)\right]\\ =&\mathcal{O}\left(\Delta x\right) + \mathcal{O}\left(\Delta t\right)\end{aligned}$$

Thus the truncation error is dominated by and $\mathcal{O}(\Delta t)$ and $\mathcal{O}(\Delta x)$ term, so the method is first order accurate. Note that for the Crank-Nicolson method (when $\theta = \frac{1}{2}$) the method becomes second order in the time.

3.4.2. Stability

A numerical method $\mathcal{N}$ is stable when for each time T , there is a constant C such that

$$||\mathcal{N}_n|| \leq C \tag{29}$$

for all $n \leq N = T/\Delta t$, i.e., the nth power of the operator $\mathcal{N}$ is uniformly bounded up to this time. For linear difference equations, stability analysis is often particularly easy in the 2-norm, since Fourier analysis can then be used to simplify the problem. This is the basis of von Neumann stability analysis [13]. For that, an arbitrary single wave number ξ is considered and data of the form

$$Q_I^n = e^{j\xi I\Delta x}Q^n \tag{30}$$

where $j = \sqrt{-1}$. Substituting this into the numerical method results in $g(\xi, \Delta x, \Delta t)$. Then requiring that $|g(\xi, \Delta x, \Delta t)| \leq 1$ for all ξ gives a sufficient condition for stability [13]. In fact it suffices to have $|g(\xi, \Delta x, \Delta t)| \leq 1 + \alpha\Delta t$ for some constant α independent of ξ. Reorganising the numerical method results in:

$$\begin{aligned}
\alpha Q_i^{n+1} =&(1-\theta)\frac{\Delta t}{\Delta x^2}\beta Q_{i+1}^n + \left(\alpha - (1-\theta)\left(\frac{2\beta\Delta t}{\Delta x^2} - \frac{\Delta t}{\Delta x}\gamma - \Delta t\epsilon\right)\right)Q_i^n \\
&+ (1-\theta)\left(\frac{\Delta t}{\Delta x}\gamma + \frac{\Delta t}{\Delta x^2}\beta\right)Q_{i-1}^n \\
&+ \theta\frac{\Delta t}{\Delta x^2}\beta Q_{i+1}^{n+1} + \left(\theta\left(\frac{2\beta\Delta t}{\Delta x^2} - \frac{\Delta t}{\Delta x}\gamma - \Delta t\epsilon\right)\right)Q_i^{n+1} \\
&+ \theta\left(\frac{\Delta t}{\Delta x}\gamma + \frac{\Delta t}{\Delta x^2}\beta\right)Q_{i-1}^{n+1} \\
=&(1-\theta)AQ_{i+1}^n + (\alpha - (1-\theta)B)Q_i^n + (1-\theta)CQ_{i-1}^n + \theta AQ_{i+1}^{n+1} + \theta BQ_i^{n+1} + \theta CQ_{i-1}^{n+1}
\end{aligned}$$

In which $A = \frac{\Delta t}{\Delta x^2}\beta$, $B = \left(\frac{2\beta\Delta t}{\Delta x^2} - \frac{\Delta t}{\Delta x}\gamma - \Delta t\epsilon\right)$ and $C = \left(\frac{\Delta t}{\Delta x}\gamma + \frac{\Delta t}{\Delta x^2}\beta\right)$. Substitution now results in:

$$\begin{aligned}
\alpha Q^{n+1}e^{j\xi i\Delta x} =&(1-\theta)AQ^n e^{j\xi(i+1)\Delta x} + (\alpha - (1-\theta)B)Q^n e^{j\xi i\Delta x} + (1-\theta)CQ^n e^{j\xi(i-1)\Delta x} \\
&+ \theta AQ^{n+1}e^{j\xi(i+1)\Delta x} + \theta BQ^{n+1}e^{j\xi i\Delta x} + \theta CQ^{n+1}e^{j\xi(i-1)\Delta x}
\end{aligned}$$

Division by $e^{j\xi i\Delta x}$ results in:

$$\begin{aligned}
\alpha Q^{n+1} =&(1-\theta)AQ^n e^{j\xi\Delta x} + (\alpha - (1-\theta)B)Q^n + (1-\theta)CQ^n e^{-j\xi\Delta x} \\
&+ \theta AQ^{n+1}e^{j\xi\Delta x} + \theta BQ^{n+1} + \theta CQ^{n+1}e^{-j\xi\Delta x}
\end{aligned}$$

Rewritten as:

$$\begin{aligned}
(\alpha - \left(\theta Ae^{j\xi\Delta x} + \theta B + \theta Ce^{-j\xi\Delta x}\right))Q^{n+1} = \\
\left((1-\theta)Ae^{j\xi\Delta x} + (\alpha - (1-\theta)B) + (1-\theta)Ce^{-j\xi\Delta x}\right)Q^n
\end{aligned}$$

or

$$Q^{n+1} = \frac{\left((1-\theta)Ae^{j\xi\Delta x} + (\alpha - (1-\theta)B) + (1-\theta)Ce^{-j\xi\Delta x}\right)}{\alpha - (\theta Ae^{j\xi\Delta x} + \theta B + \theta Ce^{-j\xi\Delta x})}Q^n$$

So the amplification factor is given by:

$$g(\xi, \Delta x, \Delta t) = \frac{1 + \frac{1}{\alpha}((1-\theta)Ae^{j\xi\Delta x} - (1-\theta)B + (1-\theta)Ce^{-j\xi\Delta x})}{1 - \frac{1}{\alpha}(\theta Ae^{j\xi\Delta x} + \theta B + \theta Ce^{-j\xi\Delta x})} \tag{31}$$

For the fully explicit scheme, where $\theta = 0$, this factor becomes $g(\xi, \Delta x, \Delta t) = \frac{1}{\alpha}(Ae^{j\xi\Delta x} + \alpha - B + Ce^{-j\xi\Delta x})$. Now requiring $|g(\xi, \Delta x, \Delta t)| \leq 1$ results in stability. The triangle inequality gives:

$$|g(\xi, \Delta x, \Delta t)| = |\frac{1}{\alpha}(Ae^{j\xi\Delta x} + \alpha - B + Ce^{-j\xi\Delta x})| \leq \frac{1}{\alpha}(|A| + |\alpha - B| + |C|) \leq 1 \tag{32}$$

It is not very trivial that this factor is smaller than unity because γ can be smaller than zero. From the definition of A, B and C it can be seen that the values depend on ratio's of Δx and Δt. Requiring Δt to be of the same order as Δx^2 results in $\frac{\Delta t}{\Delta x}$ and $\frac{\Delta t}{\Delta x^2}$ not exploding. From the parameter values it then follows that the numerical method is stable. When advection is dominant it suffices for Δt to be of the same order of Δx.

On the other hand, for the fully implicit case, when $\theta = 1$, the amplification factor becomes: $g(\xi, \Delta x, \Delta t) = 1/\left[1 - \frac{1}{\alpha}(Ae^{j\xi\Delta x} + B + Ce^{-j\xi\Delta x})\right]$. Now requiring $|g(\xi, \Delta x, \Delta t)| \leq 1$ results in $|1 - \frac{1}{\alpha}(Ae^{j\xi\Delta x} + B + Ce^{-j\xi\Delta x})| \geq 1$. Substitution of A, B and C in the inequality results in:

$$\left|1 - \frac{1}{\alpha}\left(\frac{\Delta t}{\Delta x^2}\beta e^{j\xi\Delta x} + \left(\frac{2\beta\Delta t}{\Delta x^2} - \frac{\Delta t}{\Delta x}\gamma - \Delta t\epsilon\right) + \left(\frac{\Delta t}{\Delta x}\gamma + \frac{\Delta t}{\Delta x^2}\beta\right)e^{-j\xi\Delta x}\right)\right| \geq 1$$

Reorganising and usage of $e^{-jx} + e^{jx} = 2\cos(x)$ results in:

$$\left|1 - \frac{1}{\alpha}\left(\frac{2\Delta t}{\Delta x^2}\beta\cos(\xi\Delta x) + \frac{2\beta\Delta t}{\Delta x^2} - \frac{\Delta t}{\Delta x}\gamma - \Delta t\epsilon + \frac{\Delta t}{\Delta x}\gamma e^{-j\xi\Delta x}\right)\right| \geq 1$$

Now Euler's formula gives:

$$\left|1 - \frac{1}{\alpha}\left(\frac{2\Delta t}{\Delta x^2}\beta\cos(\xi\Delta x) + \frac{2\beta\Delta t}{\Delta x^2} - \frac{\Delta t}{\Delta x}\gamma - \Delta t\epsilon + \frac{\Delta t}{\Delta x}\gamma\cos(-\xi\Delta x)\right) - \frac{\Delta t}{\alpha\Delta x}\gamma j\sin(-\xi\Delta x)\right| \geq 1$$

So the length is given by:

$$\sqrt{\left(1 - \frac{\Delta t}{\alpha\Delta x}\left(\frac{2\beta}{\Delta x} - \gamma - \Delta x\epsilon + \left(\frac{2\beta}{\Delta x} + \gamma\right)\cos(\xi\Delta x)\right)\right)^2 + \left(\frac{\Delta t}{\alpha\Delta x}\gamma\sin(-\xi\Delta x)\right)^2}$$

Requiring this length to be larger than one results in stability. Implementing this in MATLAB for $\xi \in [0, 2\pi]$ in a breathing period results in a length larger than one for $\Delta t = 0.1s$. This will be used in the present work.

4. Results

The goal of this thesis is to calculate the deposition fraction for particles with varying particle diameter d. In the previous section the equation describing the concentration of the aerosols, equation (4), was numerically solved resulting in equation (27). With this equation it is possible to calculate the concentration of particles, with a certain diameter d, in each generation of Weibel's model and in each time in a breathing cycle. Section 2.5 showed that the deposition fraction can be calculated from the concentration profile of a breathing period.

In this section the results of the present work will be compared with experimental and numerical work of others. When satisfactory agreement is obtained, a series of parameter studies will be performed by changing breathing conditions, particle parameters and lung geometries.

All the simulations will be done with a time step of $\Delta t = 0.1$s and a grid size of 481 nodes, 20 nodes equally spaced in each generation and one extra in the first generation. Since the length of an airway decreases for larger generations, the distance between the nodes also decreases for larger generations. Besides that, symmetric breathing over a breathing period of $T = 4s$ with tidal volume $V_T = 1000cm^3$ and lung volume at rest $V_{FRC} = 3300cm^3$ will be considered.

4.1. Comparison with literature

The deposition fraction per generation length and the total deposition fraction (sum of all generation) will be calculated for aerosol particles with diameter ranging from $0.01\mu m$ to $10\mu m$. In order to check the validity, the results will be compared with numerical results of Mitsakou, Helmis, and Housiadas [1] and experimental results of Lippmann [14], Chan and Lippmann [15] and Stahlhofen, Gebhart, and Heyder [16]. Before that the concentration and velocity profile are analysed.

4.1.1. Velocity and concentration profile

In section 3.4 the equation describing the velocity profile, equation (16), was obtained from the continuity equation. With this equation the velocity can be calculated in every generation at any time during a respiration cycle. The total cross sectional area, A_A can be calculated from Weibel's data and the lung volume is described with equation 1. The time derivatives and the integral were calculated with numerical functions in Matlab, respectively 'gradient' and 'trapz'.

The velocity profile at different times in a breathing period of 4 seconds is plotted in Figure 3. Note that the velocity is largest after 1 second, halfway the inspiration phase. This is totally expected since the velocity is proportional to the time derivative of the lung volume, which is taken as a cosine. Also the velocity is highest in generation three, this is because the total cross sectional area is smallest there. The velocity approaches zero for larger generations which is due to enormous increase of total cross sectional area. From generation 16 and larger the cross sectional area becomes times dependent which results in the integral in equation (16) being nonzero. This value turned out to be very small which resulted in a (almost) constant velocity in every generation.

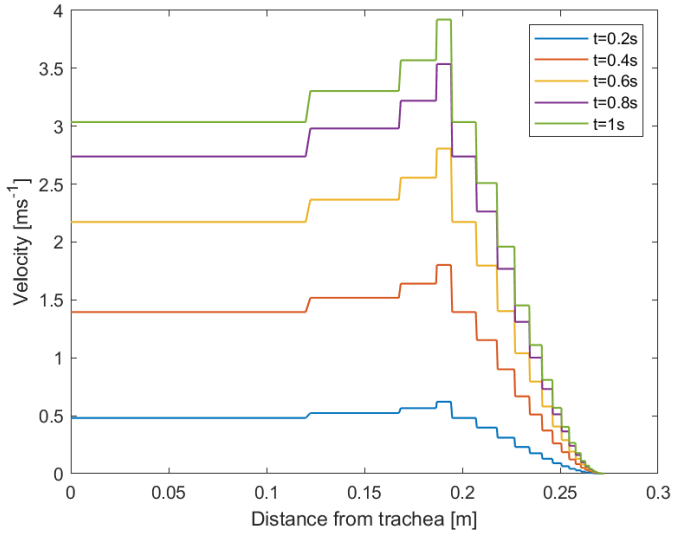

Figure 3: Velocity in $\frac{m}{s}$ plotted against the distance from the trachea (beginning of the RT) for different times during symmetric breathing. After one second in the inspiration phase the velocity reaches its maximum.

From the velocity profile it is possible to calculate the Reynolds number. This is plotted for different times during the inspiration phase in Figure 4. Just like the velocity, the Reynolds number is largest halfway the inspiration phase, after 1 second. This maximum is reached in the first generation with a value of just over 3000. Since air flow is laminar when the Reynolds number is smaller than 2300, it follows that the air flow is laminar in all generations but the first.

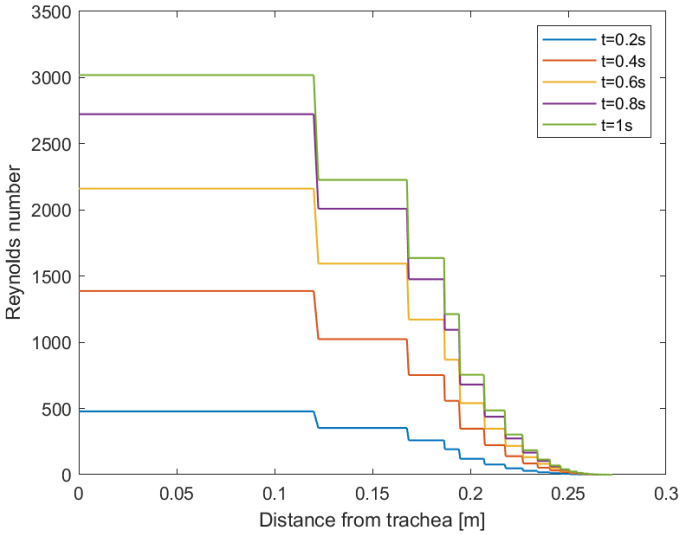

Figure 4: Reynolds number is plotted against the distance from the trachea for different times during symmetric breathing. Just like the velocity profile, the Reynolds number reaches its maximum half way the inspiration phase.

By solving the GDE, equation (4), the concentration at every generation and any time is

obtained. In section 4.1 this equation was numerically deduced to equation (27) with which the concentration can be calculated iteratively for every moment in a breathing period. Note that the deposition of particles highly depends on the particle diameter. In general it is expected that smaller particles will penetrate deeper into the RT than larger particles.

In Figure 5 the normalized concentration at different times during inspiration and expiration is plotted. The time step between the different curves is 0.2s and in total there are ten curves in the each figure. Ultrafine aerosols with diameter $d = 0.05\mu$m are considered. From the left figure it follows that the normalized concentration rises fast form 0 to 1 over a major part of the lung. However, the concentration rises very little in the last generations. This effect is a result of the velocity approaching zero for these generations. From the right figure it follows that the concentration aerosols decreases quickly in the during expiration to zero, resulting in steady breathing.

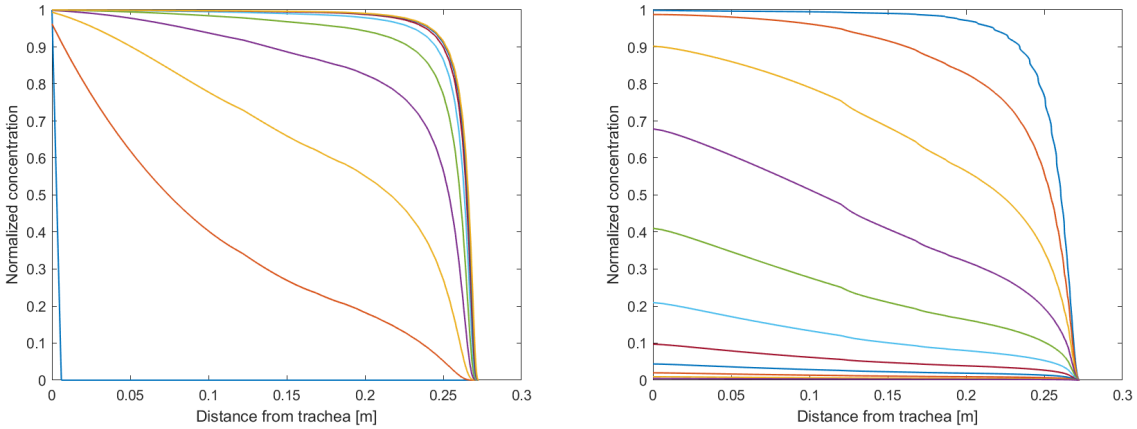

(a) Inspiration (b) Expiration

Figure 5: Normalized aerosol concentration plotted against the distance from the trachea during inspiration and expiration. The time step between the different curves is 0.2s and in total there are ten curves in the each figure.

4.1.2. Deposition fraction

The goal of this thesis is to calculate the deposition fraction for different aerosol diameters d. The diameter of these aerosol particles range from 0.01 μm to 10 μm. The deposition fraction is calculated with (17) together with the numerical integration function 'trapz' of MATLAB. This function approximates an integral via the trapezoidal method.

First the total deposition fraction (sum over the whole of the RT) is compared with numerical results of [1]. This comparison is plotted in Figure 6 for $\rho_p = 500$ kg/m^3 and $\rho_p = 1000$ kg/m^3. From both plots it follows that the deposition fraction is higher than 0.9 for particles with diameter $d < 10^{-8}$m and $d > 10^{-5}$m. This implies that most of the introduced aerosols with these diameters deposit in the RT. On the other hand, particles with diameter d between $10^{-7}\text{m} \leq d \leq 10^{-6}$m have a much lower change of depositing in the RT.

The results of [1] and the present work match pretty closely, even though [1] includes the effect of growth and coagulation. However, for particles with diameter $d > 10^{-6}$ the present work seems to overestimate the work of [1]. This offset could be explained by differences in

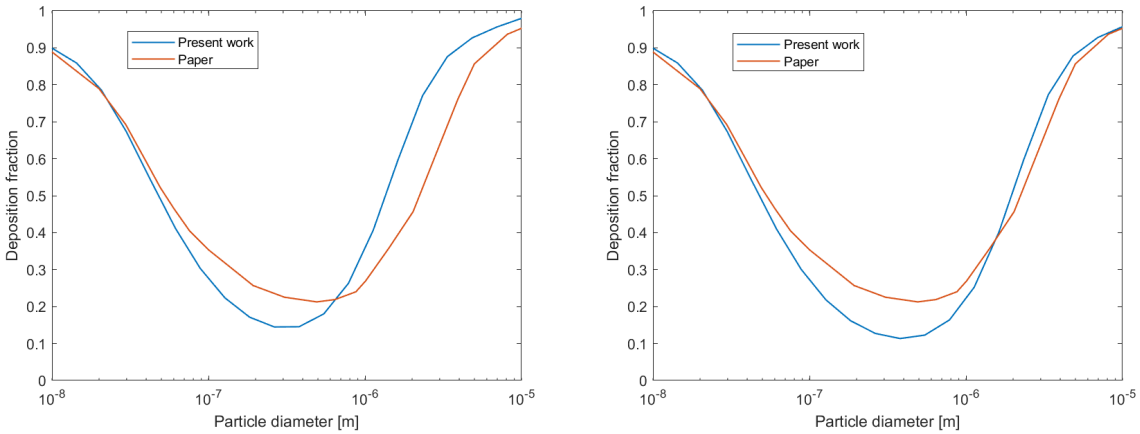

(a) $\rho_p = 1000$ kg/m^3 (b) $\rho_p = 500$ kg/m^3

Figure 6: Comparison of the total deposition fraction with numerical results of [1] for particle density $\rho_p = 1000$ kg/m^3 on the left and $\rho_p = 500$ kg/m^3 on the right.

parameter values. The numerical work of Mitsakou et al does not specify the parameter values. One constant of which the value is not very trivial is the particle density ρ_p. When bringing back the particle density to $\rho = 500$kg/m^3 instead of $\rho = 1000$kg/m^3, this overestimating gets smaller. See section 4.2.2. for detailed analysis on the influence of the particle density on the deposition fraction.

On the other hand, for particles with diameter d between 10^{-7}m and 10^{-6}m the present model underestimates the work of [1]. This offset could also be explained by a difference in Brownian diffusion coefficient D_B. When increasing D_B by 50 percent this overestimation gets smaller, see Figure 7.

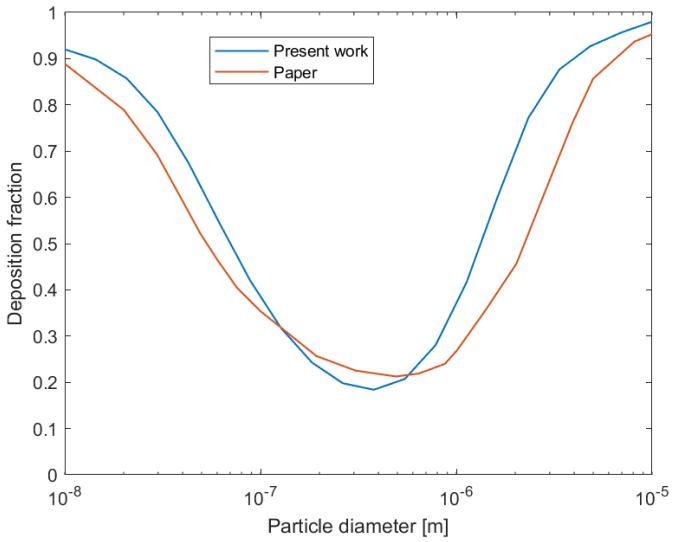

Figure 7: Total deposition fraction for increased diffusion coefficient, a particle density of $\rho_p = 1000$ is used.

Nevertheless the results of the present work and [1] never match perfectly. This could be

due to not considering the growth term in the present work. Results of [1] showed that the influence of the growth term on particle deposition is significant.

The contribution of each individual deposition mechanism, sedimentation, diffusion, impaction, to lung deposition is shown in Figure 8. From the figure it follows that deposition of ultrafine particles (diameter smaller than 0.1 μm is undertaken exclusively by diffusion, whereas coarse particles (diameter larger than 1 μm are deposited predominantly by sedimentation and impaction.

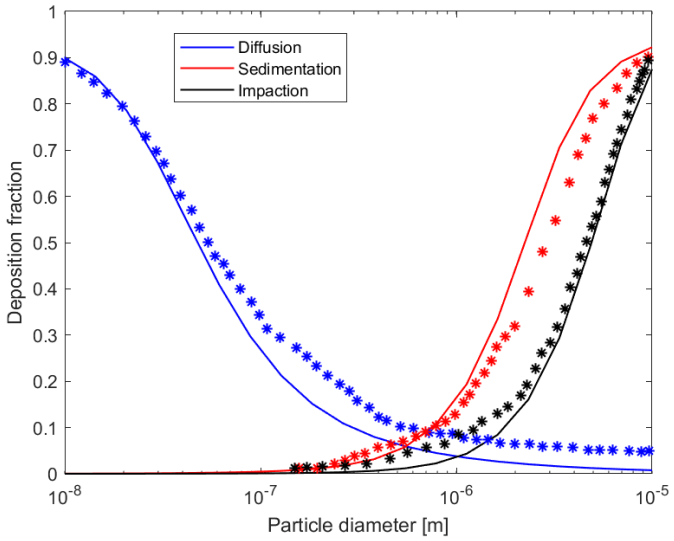

Figure 8: The contribution of each individual deposition mechanism (sedimentation, diffusion, impaction) to lung deposition compared to the results of Mitsakou et al [1]. The lines are the results of the present work and the start the results of the article.

The individual deposition mechanisms match pretty close with the results of the article. However, the deposition due to diffusion of the present work underestimates the results of [1], especially for particles with larger diameter.

Besides the total deposition fraction, it is also possible to calculate the local deposition fraction per generation. This is plotted in Figure 9 for particles with diameter $d = 0.01\mu$m and $d = 1\mu$m.

The local deposition fraction for particles with diameter $d = 0.01\mu$m match closely with the results of [1]. Both plots have a maximum close to 0.1 and approach zero for the first and last generations. However they differ in which generation the deposition is maximum. The present work seems to underestimate the work of [1] until generation 16 and overestimate from generation 17 onward. From fig 8 it follows that this could be due to a difference of the diffusion velocity, which especially affects particles with smaller diameters.

The local deposition fraction for particles with diameter $d = 1\mu$m seems to overestimate the results of [1] a bit. The overestimation in generation 1 to 10 is due to an overestimation of the impaction velocity. When the particle density is lowered to $\rho_p = 500$ this overestimation gets smaller. However it does not disappear. A difference in velocity field could be a difference for this overestimation, the impaction velocity is namely proportional to the square of the velocity. Also, the impaction velocity is proportional to the branching angle. When for example the data of Yeh and Schum is used the impaction velocity decreases. The overestimation in generation

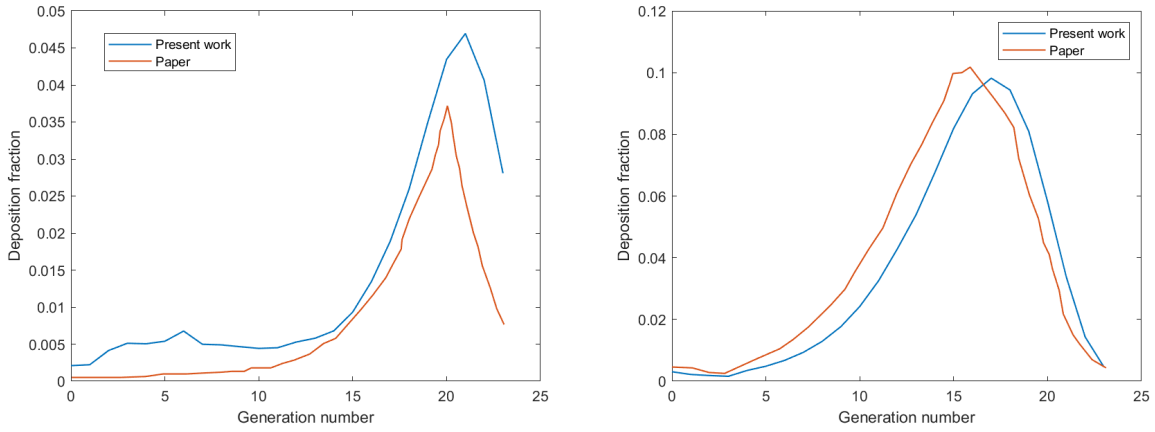

(a) $d = 1\mu m$ (b) $d = 0.01\mu m$

Figure 9: Comparison of the local deposition fraction with the article for particle with diameter $d = 0.01\mu$m on the right and $d = 1\mu$m on the left.

18 to 23 is due to an overestimation of the sedimentation velocity. Again, this could be due to differences in parameter values. By lowering the particles density the local deposition fraction matches better with the article. Similar to the impaction veolicty, the sedimentation velocity is proportional to the gravitational angle. A difference is these angles used can be a reason for the overestimation. See Figure 10 for the local deposition for particles with $\rho_p = 700$kg/m^3. Deposition in generation 13 until 20 now match really good with the results of the article. The overestimation in the other generation gets smaller, but it does not vanish.

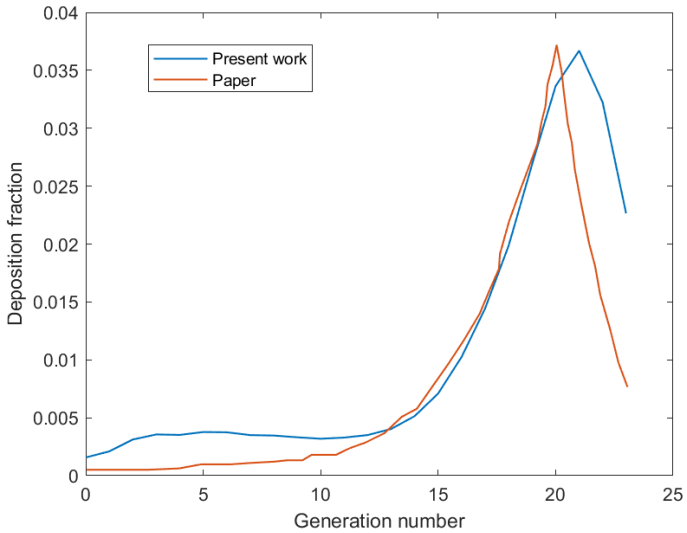

Figure 10: Local deposition fraction for particles with diameter $d = 1\mu$m and $\rho_p = 700$.

A great deal of effort has been devoted to the validation of the developed model by comparing with available experimental. Figure 11 compare the experimental results of Lippmann [14], Chan and Lippmann [15] and Stahlhofen, Gebhart, and Heyder [16] with the predictions of the present model. The data refer to deposited fractions of the tracheobronchial region (gen-

eration 0 until 17) and alveolar region (generation 17 onward). The experimental results have been obtained from in vivo measurements by non-smoker volunteers and from measurements in hollow casts of the human respiratory tree.

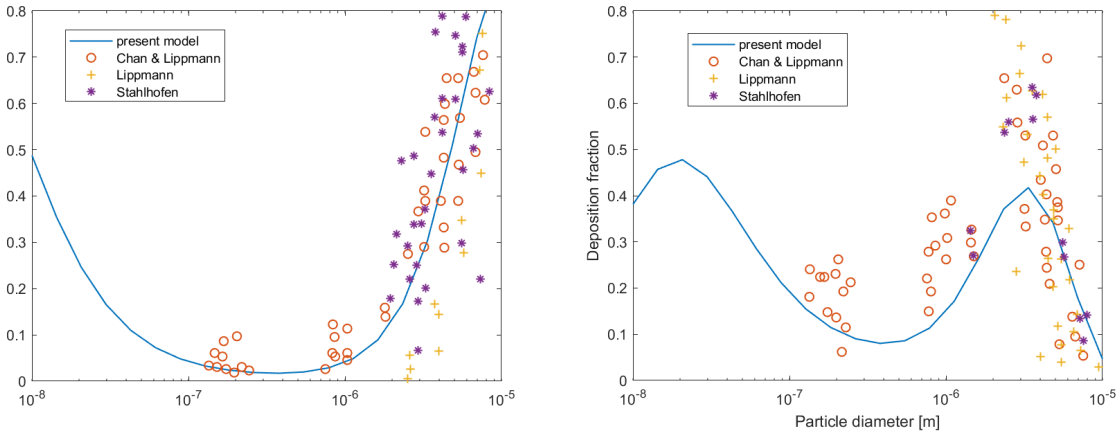

(a) Tracheobronchial region

(b) Alveolar region

Figure 11: Deposited fraction of the amount entering the trachea as a function of particle diameter, as experimentally determined and calculated in the tracheobronchial region (left) and alveolar region (right).

The present model is in agreement with the experimental data, considering the scatter in the experimental data. Especially the results in the tracheobronchial region match the experimental data very good. In the alveolar region the present work underestimates the experimental data. This underestimation can be evidence that Weibel's lung geometry is less accurate in the alveolar region than in the tracheobronchial region. Instead of the 23 generations in Weibel's model it could be that humans have more generations which would result in more deposition.

4.2. Parameter Studies

The agreement of the present work with numerical results of [1] and experimental results of [14] [15] [16] in the previous section gives the confidence that the present model performs well under a range of different conditions. In this section results of the effect of varying breathing conditions, aerosol parameters and lung geometries on the deposition fraction will be shown. This will all be done for aerosol particles with diameters ranging from 0.01μm to 10μm. This section is concluded with the mesh dependency of the total deposition fraction.

4.2.1. Breathing conditions

In this section the deposition fraction will be investigated for different breathing conditions. The breathing parameters that will be investigated are the tidal volume V_T and the breathing period T. The tidal volume is the amount of air that moves in or out of the lungs with each respiratory cycle. In rest this volume generally is between 500 and 1000 ml. Under exercise this volume can increase up to 2000 ml. A higher tidal volume results in a higher velocity in the RT, this follows directly from equation (1) and (16). It is expected that the deposition due

to impaction will mostly be influenced by a varying velocity. In Figure 12 the total deposition fraction is plotted for different tidal volumes.

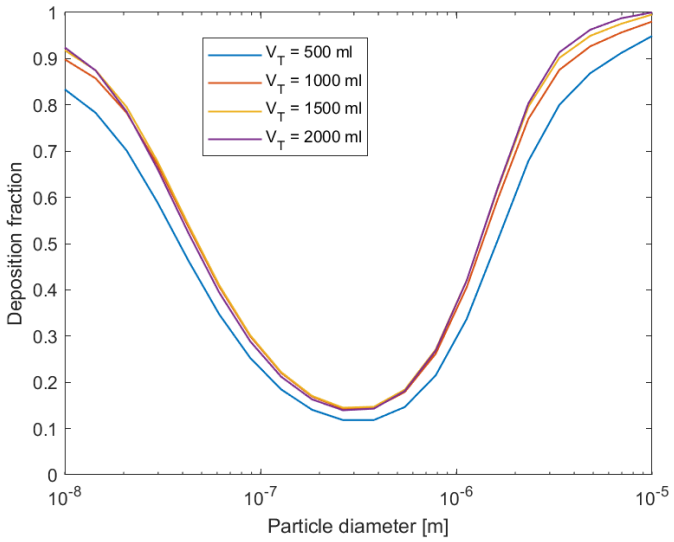

Figure 12: Total deposition fraction for different Tidal Volume's ranging from 500 to 2000 ml.

The deposition fraction does not change a lot due to varying tidal volume, especially the curves representing 1000 ml, 1500 ml and 2000 ml are really close to each other. This difference in largest between 500 and 1000 ml. As expected, the deposition due to impaction changes most for different tidal volumes, see Figure 21 in the appendix. Although the deposition fraction does not change a lot due to varying tidal volume, the total deposition will off course increase with increase tidal volume, since more particles are introduced in the RT.

The breathing period T is the time it takes for inspiration and expiration, one breathing cycle. In general when one exercises the breathing period will decrease. In rest the breathing period is typically between 4 and 5 second (or 15 to 12 breaths a minute), during exercise or hyperventilation it can be as low as 1 second (or 60 breaths a minute). The total deposition fraction for different breathing periods is plotted in Figure 13.

The deposition fraction generally decreases for decreasing breathing period (or increasing breath rate). Particles with diameter smaller than 1 μm are most influenced by this. This result may seems contradictory to the results of varying tidal volume. However, varying the breathing period between 1 and 5 seconds has an much greater influence on the velocity profile than varying the tidal volume between 500 and 2000 ml. When increasing the tidal volume to 3000 ml (which is unrealistic), the total deposition fraction will also decrease in similar manner as when the breathing period is decreased. To better visualize this, see Figure 22 in the appendix. The difference between increasing the tidal volume and decreasing the breathing period if that when the tidal volume is increased the airway diameter with alveoli also increases, see equation (2). This does not happen when the breathing period is decreased. As with the tidal volume, the total deposition will increase with decreasing breathing period, since more particles are then introduced.

This section is concluded with showing what the influence of exercise is on the deposition fraction. A breathing period of 4 seconds and tidal volume of 1000 ml is considered as normal breathing, and a breathing period of 2 seconds and tidal volume of 2000 ml is considered as

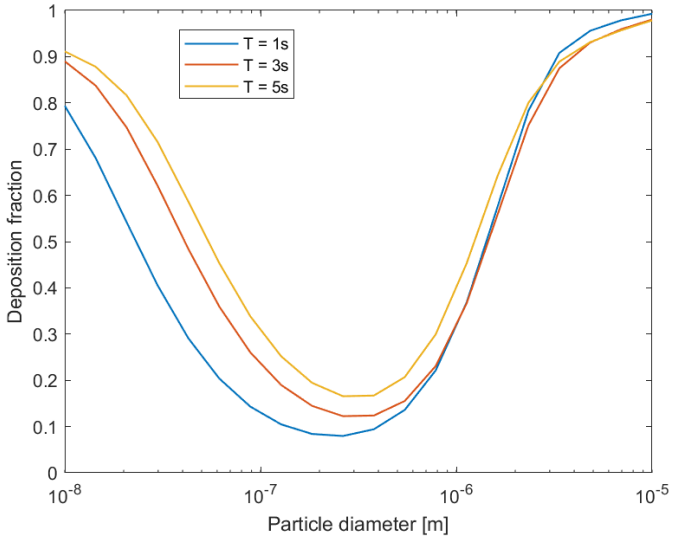

Figure 13: Total deposition fraction breathing periods T ranging from 1 to 5 second, or 60 to 12 breaths a minute.

breathing during exercise. This difference is plotted is Figure 14. From the figure it follows that the deposition fraction increases during exercise for particles with diameter between 1μm and 10μm, while the deposition fraction decreases for particles with diameter between 1μm and 0.01μm.

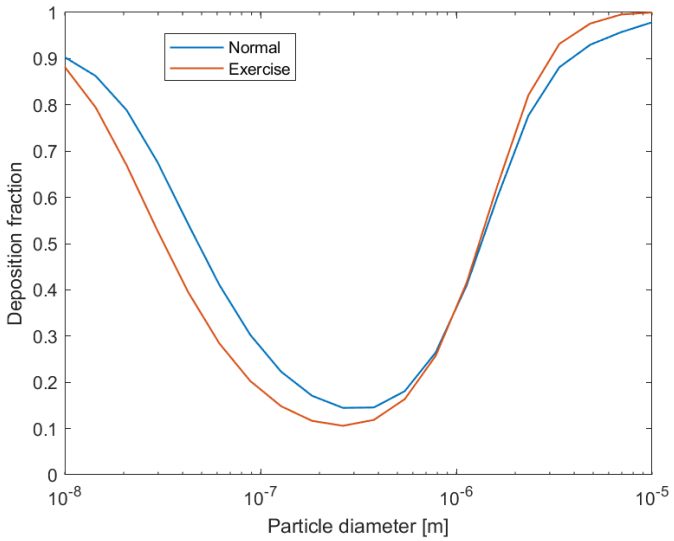

Figure 14: Comparing the total deposition fraction for normal breathing and breathing during exercise. A breathing period of 4 seconds and tidal volume of 1000 ml is considered as normal breathing, and a breathing period of 2 seconds and tidal volume of 2000 ml is considered as breathing during exercise.

4.2.2. Particle density

As discussed before the particle density influences the deposition velocity due to gravitational settling and the deposition velocity due to impaction. Since the deposition of ultrafine particles is undertaken exclusively by diffusion (see Figure 8), the total deposition is not expected to change for those ultrafine particles. The total deposition for a range of different particles density is plotted in Figure 15.

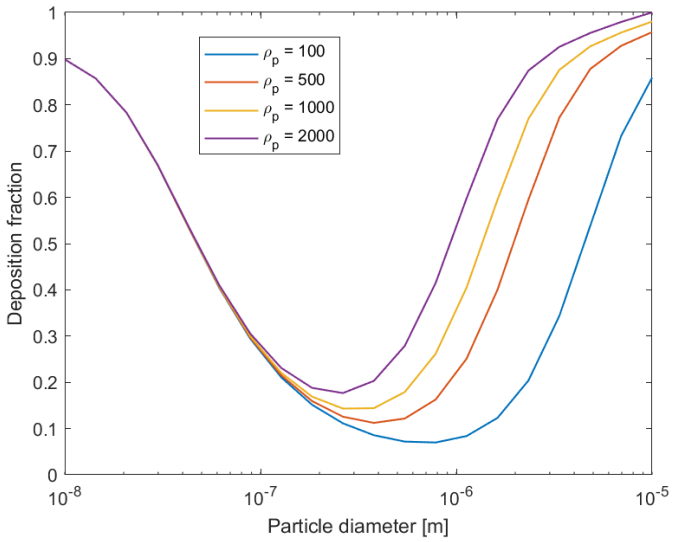

Figure 15: Total deposition fraction for different values of the particle density.

As expected the total deposition does not change for particles with diameter smaller than 0.1μm when changing the particle density. For particles with diameter larger than 0.1μm the total deposition generally gets larger for increasing particles density and shift towards the left.

4.2.3. Lung geometry

Besides Weibel's model there exists a lot of different lung models. These lung models vary in total generation number, airway diameter and length, gravitational and branching angle and possibly asymmetries. One example is the model proposed by Yeh and Schum, see Table 2 in the appendix. The lung geometry of Weibel and Yeh and Schum are compared in Figure 16.

Clearly Weibel's lung model reports a lot more deposition than Yeh and Schum's model. This difference is due to a large difference in the velocity profile between the diffent geometries. From equation (16) it follows that the velocity profile is inversely proportional to the airway diameter. Since these airway diameter differ between the two models, the velocity profile also differs, see Figure 17.

For the lower generations the velocity calculated with Weibel's model is up to 8 times larger than the velocity calculted with Yeh and Schum's model. However, the data of Yeh and Schum's used, is only a part of a more complex model. The complete model consists of six different segments, considering the difference between the right and left lung, and their top, middle and lower lobes. Each of these six segments has their own number of alveolar sacs. Implementing these corrections would result in deposition fractions similar to those calculated with Weibel's model [17].

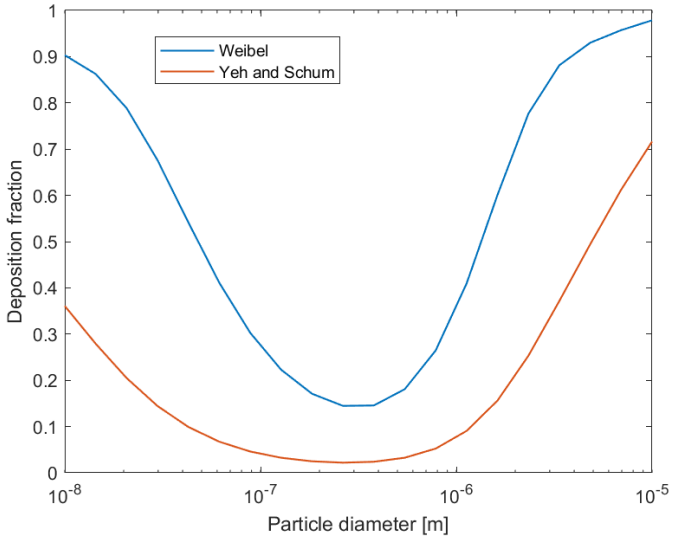

Figure 16: Comparison of the total deposition fraction calculated with Weibel's lung model and the Yeh and Schum's lung model. For the lung data see figure 1 and 2 in the aooendix.

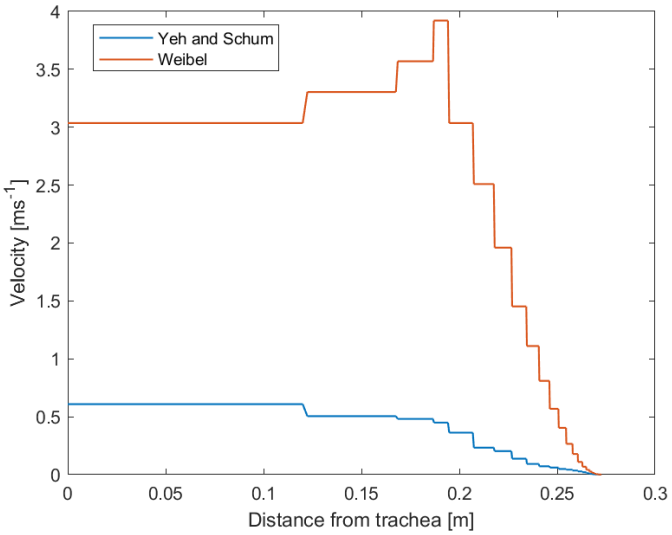

Figure 17: Comparison of the velocity profile after 1 second, halfway the inspiration phase, using Weiebl;s and Yeh and Schum's model.

Instead of changing the whole lung model it is also possible to investigate how the deposition fraction changes with (small) changes in Weibel's model. For example, one could change the airway diameter of some generation and could investigate what the effect on the total deposition fraction is. This could be relevant information for people with asthma. It is known that the airway diameter and airflow obstruction can change for people with asthma. This results in shortness of breath. In Figure 18 the deposition fraction is plotted for the standard Weibel model, and one with half airway diameter.

From Figure 18 follows that the deposition fraction increases when the diameter of the airways decrease. This increase seems to be uniform for the different particle sizes. It is not

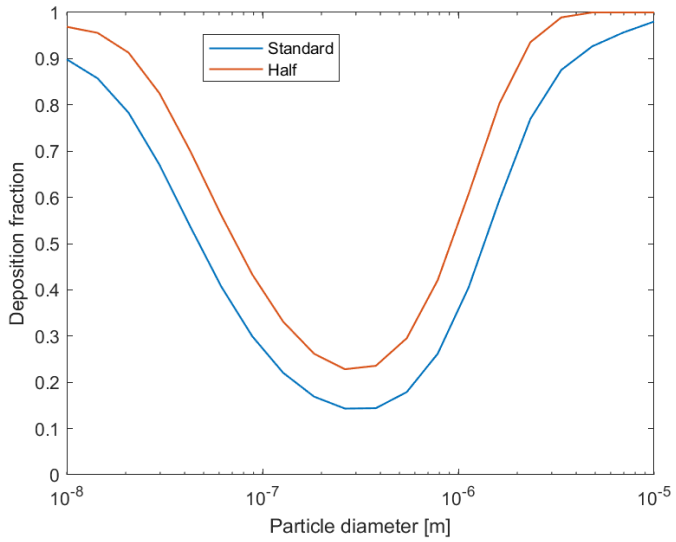

Figure 18: Total deposition fraction for the standard Weibel model and one with half the airway diameter in each generation.

very realistic that all airway diameters decrease the same amount simultaneously. Instead, the influence of a decrease in the airway diameters for the tracheobronchial and alveolar region is plotted in Figure 19.

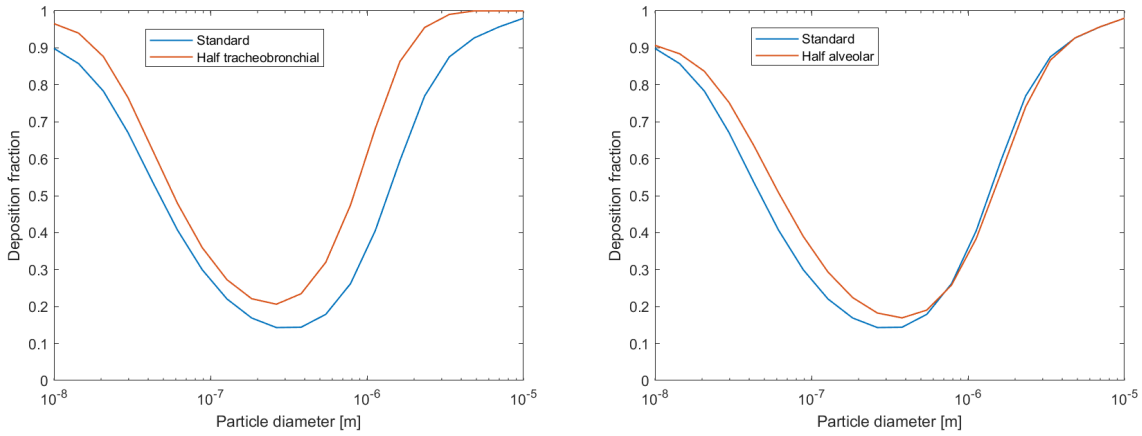

(a) Tracheobronchial regoin

(b) Alveolar regoin

Figure 19: Comparison of the total deposition fraction for the standard Weibel model and an adjusted model with half the airway diameter in the tracheobronchial region on the left and alveolar region on the right.

A decrease in airway diameter in the tracheobronchial region has a much greater influence on the total deposition fraction than an decrease in the alveolar region. It is remarkable that the deposition seems to decrease (a very little) for particles with diameter between 1 μm and 10 μm when the airway diameter in decreased in the alveolar region. Also, decreasing the airway diameter in the tracheobronchial region mostly effects aerosols with a larger diameter while decreasing the airway diameter in the alveolar region mostly effects aerosols with a smaller

diameter.

4.2.4. Mesh dependency

As stated before, all simulations have been done with a grid size of 481, 20 nodes equally spaced in each generation and one extra in the first generation. Section 3.3.1. showed that the truncation error is dominated by $\mathcal{O}(\Delta x)$ and $\mathcal{O}(\Delta t)$. Hence a difference in the number of nodes in each generation results in different errors. To investigate this difference, the total deposition fraction for a range of number of nodes in each generation is plotted in Figure 20. From the figure it follows that the curves do not differ a lot. Especially the difference between the curve for $N = 20$ and $N = 30$ is really small. Generally the deposition fraction seems to increase when the number of nodes per generation increases.

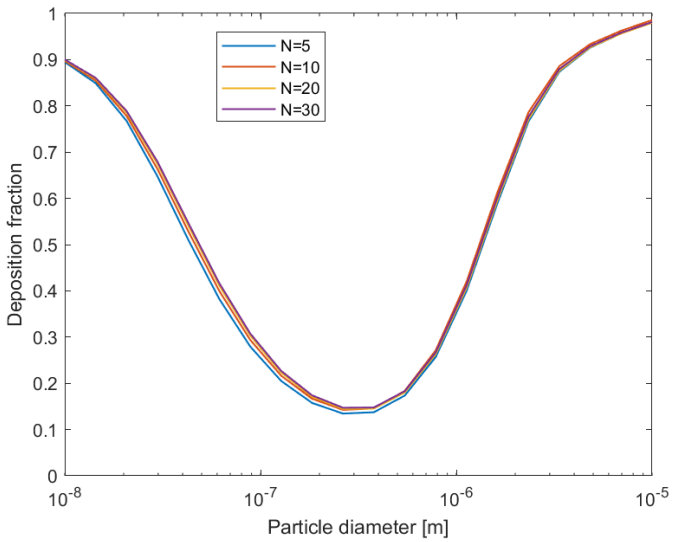

Figure 20: Total deposition fraction of a range of different nodes in each generation of Weibel's lung model.

5. Conclusion

An Eulerian model has been developed that enables determination of aerosol deposition in all generation of the respiratory tract for a range of aerosol diameters. This is done by numerically solving the aerosol general dynamic equation for a 1 dimensional lung geometry. The developed model is based on work of [1], who build a model to investigate the deposition fraction for a range of aerosol diameters. Valuation was carried out by comparing results of the model and available experimental and previous numerical results. In all comparisons satisfactory agreement was obtained.

The employed geometric lung model, although simple and symmetric, produced convincing results in terms of average deposition. Especially results of deposition in the tracheobronchial region agreed perfectly with experimental data. Of course, a more advanced lung model would be required to predict lobar, or site-specific deposition. This could be done by implementing the morphological model of Yeh and Schum in its entirety. The 1-dimensional model has been considered in this study, but the quasi 3 dimensional model would be more complete.

A series of parameter studies is performed by changing breathing conditions, particle parameters and lung geometries. An increase in Tidal volume and decrease of breathing period resulted in an increase of the total deposition fraction for coarse particles and a decrease of the total deposition fraction for ultrafine particles. Despite this, increasing the tidal volume and decreasing the breathing period results in more particle deposition, since more particles are inhales. An increase in the particle density resulted in an increase in the total deposition fraction. A decrease in the airway diameter generally resulted in an increase of the total deposition fraction. This difference was most noticeable in the tracheobronchial region. Decreasing the airway diameter in the tracheobronchial region mostly effects coarse particles while decreasing the airway diameter in the alveolar region mostly effects ultrafine particles.

Although the present model produces realistic results, there are still a lot of improvements possible for future studies. Implementation of the effects of growth and coagulation in the present model would produce even more convincing results. Besides, some debatable assumptions were made such as that the terminal settling velocity was reached instantly and that deposition due to impaction is the same during inspiration and expiration. Also, using the Crank-Nicolson method ($\theta = 1/2$) would give numerical more accurate results. For this, the time step Δt has to be of the same order as Δx^2 resulting in a longer running time.

References

[1] Christina Mitsakou, C. Helmis, and C. Housiadas. Eulerian modeling of lung deposition with sectional representation of aerosol dynamics. *Journal of Aerosol Science*, 36:75–94, 01 2005.

[2] Ewald R Weibel. Morphometry of the human lung. 1963.

[3] Bing Han and Hiroyuki Hirahara. Effect of gas oscillation-induced irreversible flow in transitional bronchioles of human lung. *Journal of Flow Control, Measurement & Visualization*, 04:171–193, 01 2016.

[4] Greene NM & Bouhuys A Scherer PW, Shendalman LH. Measurement of axial diffusivities in a model of the bronchial airways. *J Appl Physiol*, 04 1975.

[5] Chi Tien and B.V. Ramarao. 5 - trajectory analysis of particle deposition. In Chi Tien and B.V. Ramarao, editors, *Granular Filtration of Aerosols and Hydrosols (Second Edition)*, pages 169–211. Butterworth-Heinemann, Oxford, second edition edition, 2007.

[6] Ebenezer Cunningham and Joseph Larmor. On the velocity of steady fall of spherical particles through fluid medium. *Proceedings of the Royal Society of London. Series A, Containing Papers of a Mathematical and Physical Character*, 83(563):357–365, 1910.

[7] S.G Jennings. The mean free path in air. *Journal of Aerosol Science*, 19(2):159–166, 1988.

[8] Laminar flow forced convection in ducts. Academic Press, 1978.

[9] Boyun Guo and Ali Ghalambor. Natural gas engineering handbook (second edition). pages 219–262. Gulf Publishing Company, second edition edition, 2005.

[10] Dario Camuffo. Microclimate for cultural heritage (third edition). pages 197–234. Elsevier, third edition edition, 2019.

[11] Thomas Heistracher and Werner Hofmann. Physiologically realistic models of bronchial airway bifurcations. *Journal of Aerosol Science*, 26:497–509, 1995.

[12] M.Pilou, S.Tsangaris, P.Neofytou, C.Housiadas, and Y.Drossinos. Inertial particle deposition in a 90° laminar flow bend: An eulerian fluid particle approach. July 2011.

[13] Randall J. LeVeque. *Finite Volume Methods for Hyperbolic Problems*. Cambridge Texts in Applied Mathematics. Cambridge University Press, 2002.

[14] M. Lippmann. Regional deposition of particles in the human respiratory tract. *Handbook of physiology, Section 9: Reactions to environmental agents*, pages 213–232, 1977.

[15] T.L. Chan and M. Lippmann. Growth and deposition of hygroscopic particulate matter in the human lungs. *Aerosol Science and Technology*, pages 144–159.

[16] Stahlhofen W, Gebhart J, and Heyder J. Experimental determination of the regional deposition of aerosol particles in the human respiratory tract. *Am Ind Hyg Assoc J.*, pages 144–159, Jun 1980.

[17] Hsu-Chi Yeh and G.M. Schum. Models of human lung airways and their application to inhaled particle deposition. *Bulletin of Mathematical Biology*, 42(3):461–480, 1980.

6. Appendix

6.1. Lung data

Table 1: Weibel's lung data [2].

Generation Z	Number per generation $n(Z)$	Diameter $d(Z)$, cm	Length $l(Z)$ cm
0	1	1.8	12.0
1	2	1.22	4.76
2	4	0.83	1.90
3	8	0.56	0.76
4	16	0.45	1.27
5	32	0.35	1.07
6	64	0.28	0.90
7	128	0.23	0.76
8	256	0.186	0.64
9	512	0.154	0.54
10	1024	0.13	0.46
11	2048	0.109	0.39
12	4096	0.095	0.33
13	8192	0.082	0.27
14	16384	0.074	0.23
15	32768	0.066	0.20
16	65536	0.060	0.165
17	131072	0.054	0.141
18	262144	0.050	0.117
19	524288	0.047	0.099
20	1048576	0.045	0.083
21	2097152	0.043	0.070
22	4194304	0.041	0.059
23*	8388608	0.041	0.050*

* Adjusted for complete generation.

Table 2: Yeh and Schum's lung data [17].

n	Number of tubes	L (cm)	d (cm)	Θ (°)	Φ (°)
1	1	10.0	2.01	0	0
2	2	4.36	1.56	33	20
3	4	1.78	1.13	34	31
4	8	0.965	0.827	22	43
5	16	0.995	0.651	20	39
6	32	1.01	0.574	18	39
7	64	0.890	0.435	19	40
8	128	0.962	0.373	22	36
9	256	0.867	0.322	28	39
10	512	0.667	0.257	22	45
11	1024	0.556	0.198	33	43
12	2048	0.446	0.156	34	45
13	4096	0.359	0.118	37	45
14	8192	0.275	0.092	39	60
15	16,384	0.212	0.073	39	60
16†	32,768	0.168	0.060	51	60
17	65,536	0.134	0.054	45	60
18	131,072	0.120	0.050	45	60
19	262,144	0.092	0.047	45	60
20	524,288	0.080	0.045	45	60
21	1,048,576	0.070	0.044	45	60
22	2,097,152	0.063	0.044	45	60
23	4,194,304	0.057	0.043	45	60
24	8,388,608	0.053	0.043	45	60
25‡	3×10^8	0.025	0.030	45	60

6.2. Tidal volume and breathing period

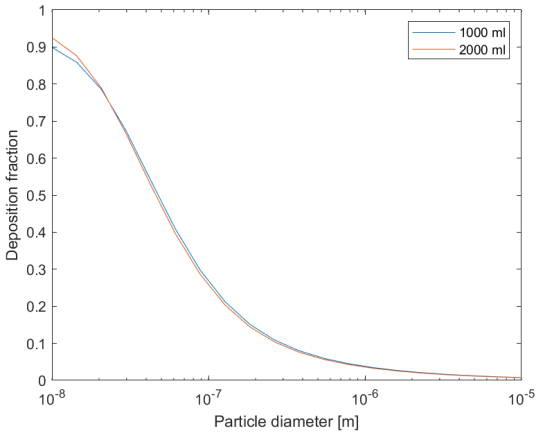

(a) Diffusion

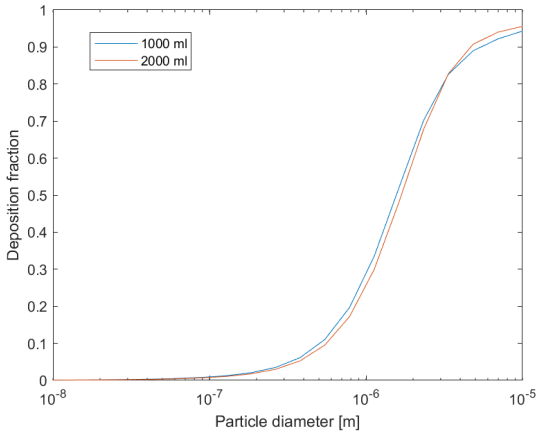

(b) Sedimentation

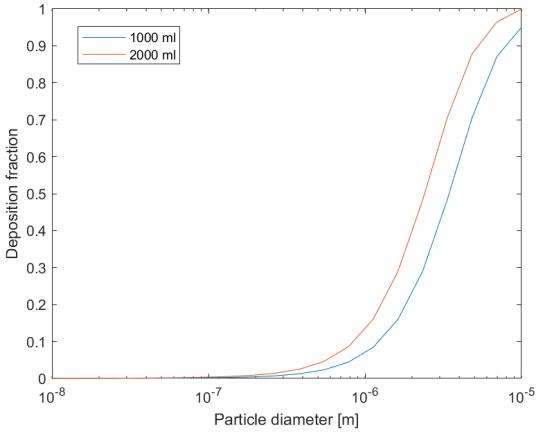

(c) Impaction

Figure 21: Total deposition fraction of each individual deposition mechanism for tidal volumes $V_T = 1000$ ml and $V_T = 2000$ ml. Deposition due to diffusion and sedimentation hardly change, while deposition due to impaction increases due to increasing tidal volume.

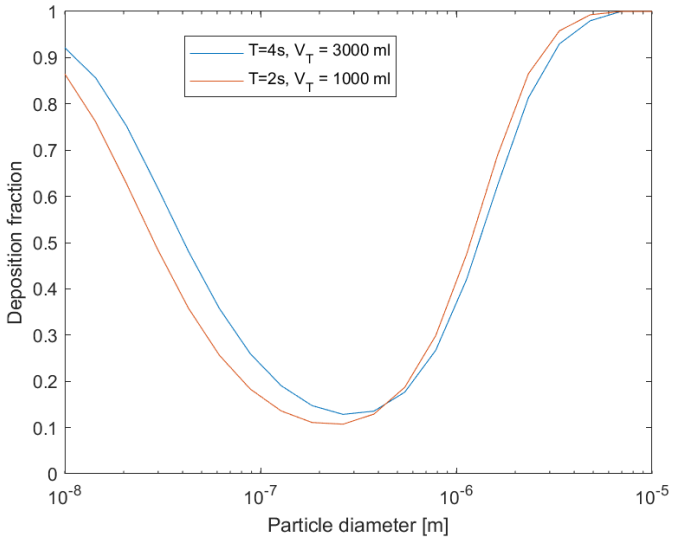

Figure 22: Comparison of total deposition fraction for breathing with breathing rate $T = 4$s and tidal volume $V_T = 3000$ ml and breathing with breathing rate $T = 2$s and tidal volume $V_T = 1000$ ml. Both curves have similar shape giving evidence that increasing tidal volume and decreasing breathing period results in similar deposition of aerosols.